Journal of Biomedical Optics 9(2), 282–286 (March/April 2004)

Use of optical coherence tomography to monitor biological tissue freezing during cryosurgery

Bernard Choi
Beckman Laser Institute
University of California, Irvine
Irvine, California 92612
E-mail: bchoi@laser.bli.uci.edu

Thomas E. Milner
Jeehyun Kim
University of Texas
Department of Biomedical Engineering
Austin, Texas 78712

Jared N. Goodman
Brigham Young University
Department of Psychology
Provo, Utah 84602

Gracie Vargas
University of Texas
Department of Biomedical Engineering
Austin, Texas 78712

Guillermo Aguilar
Beckman Laser Institute
University of California, Irvine
Irvine, California 92612
and
University of California, Riverside
Department of Mechanical Engineering
Riverside, California 92521

J. Stuart Nelson
Beckman Laser Institute
University of California, Irvine
Irvine, California 92612

Abstract. The use of optical coherence tomography (OCT) for imaging skin during cryosurgery is evaluated. OCT provides high spatial resolution (5–10 μm) images of optical backscattering due to local variations in refractive index, such as the boundary between liquid and frozen water in tissue. Time resolved OCT images were acquired during freezing of water, Intralipid™, and *in vivo* hamster skin. Subsurface morphological changes were evident only during freezing of Intralipid and skin. A simple thermal model was applied which predicted freezing times on the same order of magnitude as those observed in OCT images. OCT can be used as a feedback tool during cryosurgical procedures to monitor progression of the freezing front.
 [DOI: 10.1117/1.1648647]

Keywords: biomedical optical imaging; tissue phantoms; hamster window model; skin flap model.

Paper 014008 received Mar. 28, 2003; revised manuscript received Nov. 3, 2003, and Dec. 22, 2003; accepted for publication Dec. 22, 2003.

1 Introduction

Cryosurgery is a technique used for destruction of malignant lesions in the breast,[1,2] prostate,[3] liver,[4,5] and skin.[6] Real time localization of the freezing front boundaries is essential for optimization of cryosurgical procedures. Ultrasound[2] and magnetic resonance imaging[5] techniques have been used to provide such feedback. Otten et al.[7] used optical spectroscopy to detect the onset of the formation of ice during the freezing of muscle. We hypothesize that freezing dynamics can be monitored by optical imaging and now report on the use of optical coherence tomography (OCT) for real time, high resolution imaging feedback during freezing of tissue phantoms and an *in vivo* skin model. An advantage of OCT is that it can be incorporated easily into a variety of clinical imaging devices, including microscopes, surgical imaging probes, fiber optic endoscopes, catheters, laparascopes, and needles through which cryosurgery might be performed.

2 Materials and Methods

2.1 *OCT System*

Images were obtained using OCT, which utilizes broadband light and a modified Michelson interferometer to acquire depth- and time-resolved images of the samples under study. For more details on basic principles of OCT, the reader is directed to Refs. 8–13. Briefly, OCT is the light-based analog of ultrasound imaging. Using a superluminescent diode (SLD), broadband light experiences scattering and absorption events as it propagates through tissue. Since currently available detectors are not fast enough to differentiate between photons backscattered from different depths in tissue, an interferometric-based coherence-gated detection system is required to specify the amount of light backscattered from various depths. By scanning the probe beam laterally, a two-dimensional (2D) cross-sectional image can be obtained.

In our system, the broadband SLD (model BBS 1310 B-TS, Advanced Fiber Communications, Petaluma, CA) emitted light at a wavelength of 1310 ± 70 nm. Both axial and lateral resolutions were 10 μm. OCT image sequences were acquired at frame rates of 1 Hz. Each image consisted of 2000 depth scans, each of which consisted of 1500 samples.

2.2 *Experimental Materials*

De-ionized water and Intralipid™ (Research Biochemicals International, Natick, MA) were used as biological tissue-

1083-3668/2004/$15.00

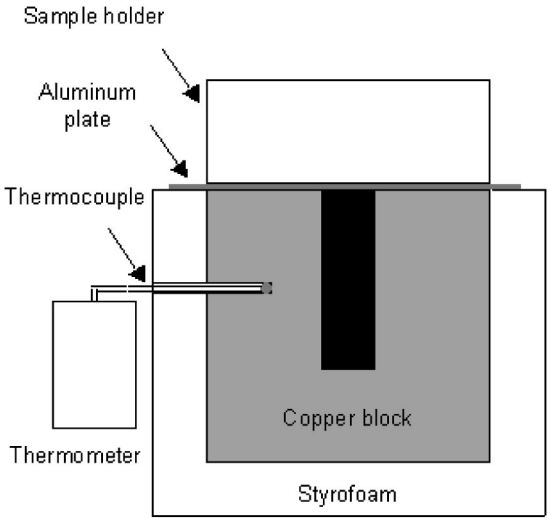

Fig. 1 Schematic of the copper block apparatus used to freeze aqueous samples.

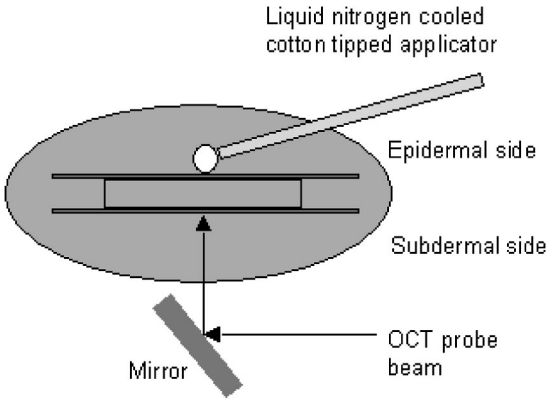

Fig. 2 Schematic of the *in vivo* hamster window chamber experimental setup.

simulating phantoms. Water was used to simulate the high water content (~70%)[14] of skin. Intralipid is a suspension of lipid globules with an appearance similar to milk that is used as a scattering medium in tissue-simulating phantoms.[15]

2.3 *Animals*

To obtain depth-resolved images of skin during cooling, the *in vivo* hamster window chamber model was used.[16–19] Briefly, surgical installation of a dorsal skin fold window permitted observation of full-thickness skin from both the epidermal and subdermal sides. A section for skin flap placement on the back of the animal was selected, surgically scrubbed, shaved, and depilated. Sutures attached to a temporary mount retracted the dorsal skin from the body. A circular section with an approximate diameter of 1 cm was cut from one side of the symmetrical skin fold, thus exposing a thin layer of subdermal skeletal muscle, blood vessels, and subcutaneous tissue of the underlying skin. An aluminum chamber was sutured to both sides of the skin. To prevent dehydration, saline was applied periodically to the subdermal skin. Hamster window surgery was performed as defined by a protocol approved by The University of Texas Animal Use Committee.

2.4 *Study Design*

To evaluate the capability of OCT to image tissue freezing during cryosurgery, we acquired OCT images during liquid nitrogen enhanced cooling of water, Intralipid, and *in vivo* hamster skin. For the first set of experiments, a block of copper (a cube with dimensions of 8 cm) was embedded in Styrofoam for thermal insulation (Fig. 1). A 1.5 cm diam, 6 cm deep cylindrical hole was created on the top surface of the copper block. A second 0.5 cm diam hole was created on the side of the copper block. A thermocouple (type K, Omega Engineering, Stamford, CT) was inserted into the second hole so that the temperature of the block could be monitored with a digital thermometer (Omega Engineering). Before the experiments were performed, the block was stored in a −80 °C freezer. In order to achieve a relatively stable block temperature of approximately −100 °C, liquid nitrogen was poured periodically into the top hole. Water or Intralipid was placed in a custom-made sample holder that consisted of two glass slides attached to a thin plate of aluminum. Feeler gauge stock (McMaster–Carr, Los Angeles, CA) was placed between the slides to achieve a gap of ~1 mm. The holder was placed on the cooled copper block and positioned such that the OCT probe beam was scanned along the length of the sample holder, over a lateral distance of 2 mm. OCT images were acquired at one image per minute.

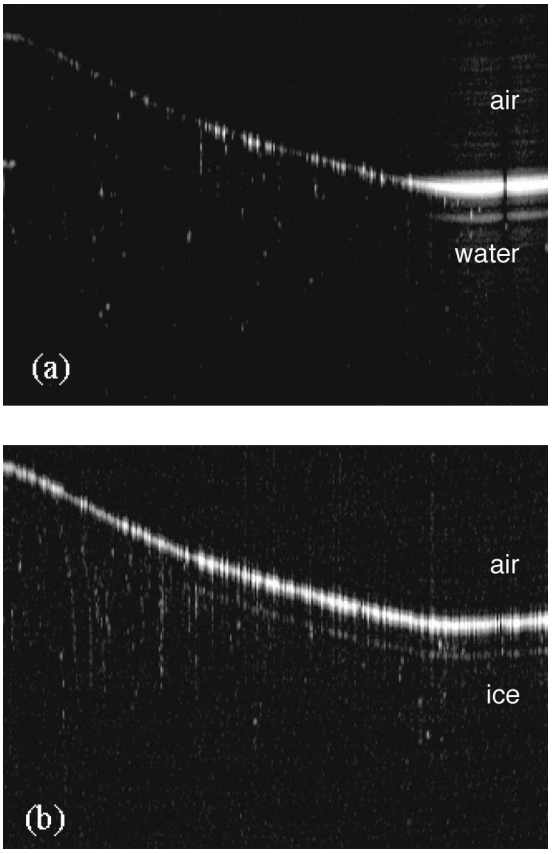

Fig. 3 OCT images of water (a) prior to and (b) after completion of the freezing process. Subsurface morphological changes were not observed during freezing.

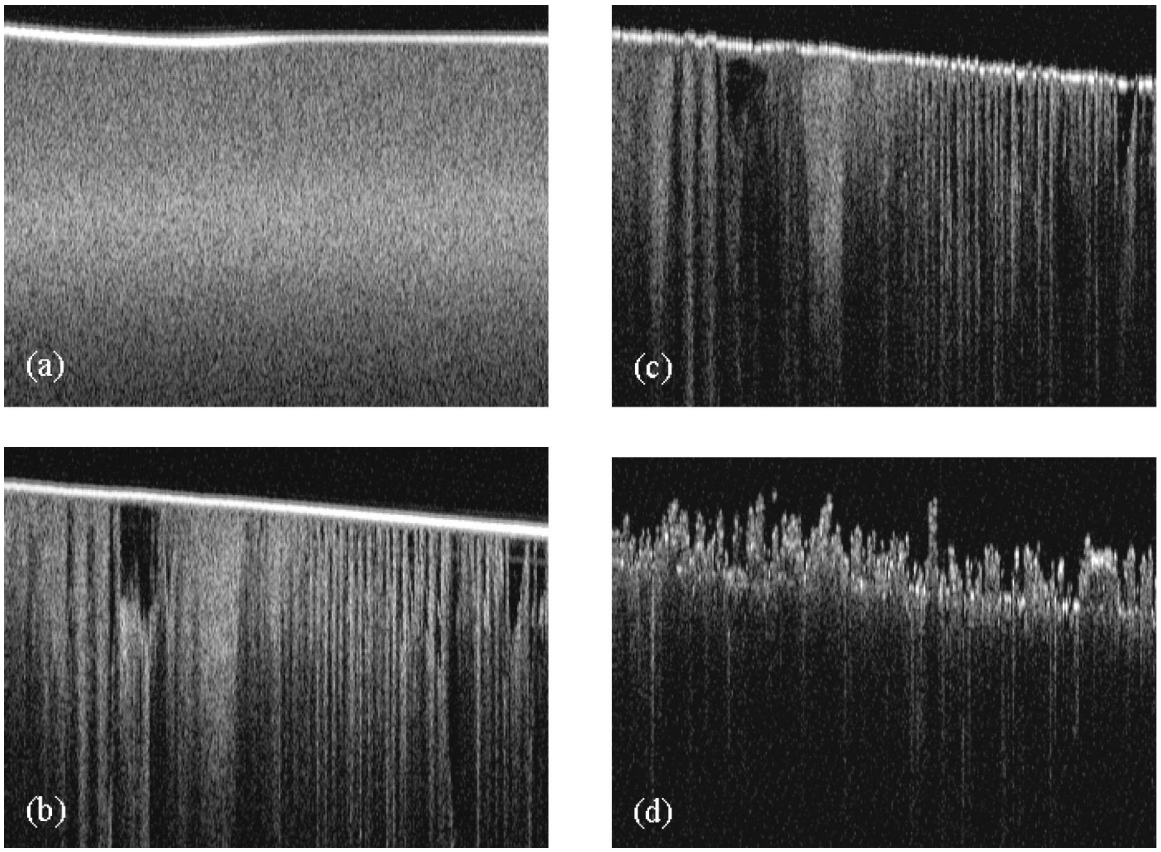

Fig. 4 OCT images of Intralipid™ (a) prior to (b), (c) during, and (d) after completion of freezing. Subsurface morphological changes were evident in (b) and (c) during freezing. (d) After freezing, subsurface features were no longer evident.

The second set of experiments involved application of a liquid nitrogen soaked cotton tipped applicator to the epidermal side of the hamster window chamber preparation (Fig. 2). The temperature of the applicator was estimated with a digital thermometer. OCT images were acquired from the subdermal side at a frame rate of 1 Hz. To store all images acquired at this frame rate, the number of *A* scans per image was reduced by a factor of 5 to satisfy acquisition bandwidth limitations.

3 Results

3.1 *Freezing of Water and Intralipid*

With water, OCT can be used to detect freezing only after the surface has frozen (Fig. 3). Figure 3(a) shows the OCT imaged surface of the water before freezing. The surface is more clearly defined in the image after freezing [Fig. 3(b)]. A freezing front progressing from the copper block top surface towards the water surface was not evident in OCT images, although small local increases in subsurface signal was observed due to reflectance off water–ice boundaries.

Prior to freezing, OCT imaging of Intralipid showed a strong surface reflectance signal with progressively decreasing signal intensity with increasing depth [Fig. 4(a)]. These characteristics are also observed in OCT images of biological tissues such as skin (Fig. 5, Refs. 8–13). As the freezing front approached the Intralipid surface, icicle-like regions of light scattering were observed [Fig. 4(b)]. As the freezing process continued, the surface reflectance increased in intensity and obscured the underlying structural morphology [Fig. 4(c)]. Once completely frozen, the Intralipid surface eventually assumed a jagged appearance [Fig. 4(d)].

3.2 *Freezing of In Vivo Hamster Skin*

Upon immersion in liquid nitrogen, the cotton-tipped applicator reached the boiling temperature of $-196\,^{\circ}\mathrm{C}$. After removal and exposure to air, the applicator tip temperature slowly increased. Over the initial 20 s, the measured temperature remained below $-100\,^{\circ}\mathrm{C}$, measured with a thermocouple-based digital thermometer. After immersion and immediate application to skin, the applicator tip temperature was approximately $-80\,^{\circ}\mathrm{C}$.

An OCT image sequence obtained while applying the cotton-tipped applicator to the epidermal surface in the absence of liquid nitrogen (i.e., control conditions) showed no gross change in OCT signal amplitude [Fig. 5(a)]. The images in Fig. 5 appear pointed due to pressure exerted by the applicator on the epidermal surface. Relative changes in skin position were due to slight movement of the experimenter's hand while applying the applicator. OCT skin cross-sectional image sequences were obtained at 1 Hz during liquid nitrogen freezing [Fig. 5(b)]. At $t=6$ s, the OCT signal amplitude at the subdermal surface increased, with corresponding decreases at regions closer to the liquid nitrogen source, due to an increase in light remitted from frozen subdermal tissue.

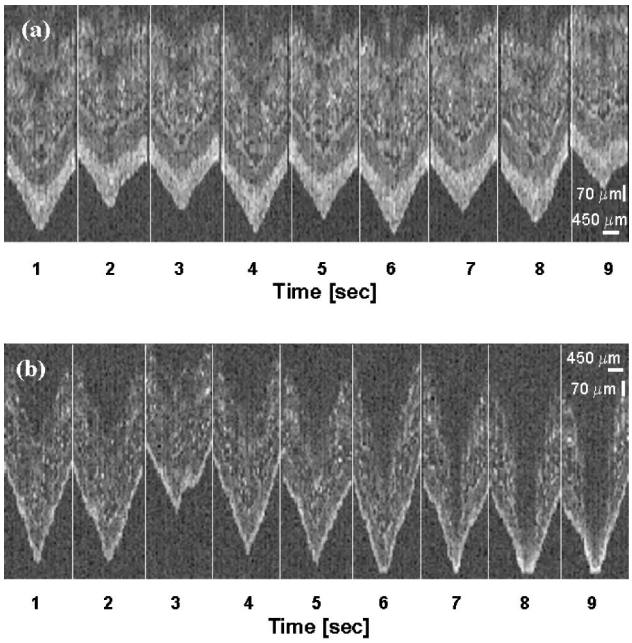

Fig. 5 (a) OCT image sequence obtained during application of the cotton-tipped applicator alone (i.e., no liquid nitrogen) to the epidermal surface. (b) OCT image sequence during contact application of liquid nitrogen to the epidermal side of the hamster window chamber. The OCT probe beam was incident on the subdermal side. At $t = 6$ s, the subdermal surface OCT signal amplitude noticeably increased, with a corresponding decrease in signal amplitude at regions closer to the liquid nitrogen source. Scale bars=70 μm (vertical); 450 μm (horizontal).

The magnitude of these changes increased with the amount of time of liquid nitrogen contact as the freezing process continued.

4 Discussion

This study on tissue phantoms and *in vivo* hamster skin demonstrates that OCT can be effective for monitoring progression of the freezing front during cryosurgery. With OCT, local variations in refractive index serve as the primary source of contrast. In most biological tissues, the primary constituents are water and collagen. At the SLD source wavelength of 1310 nm, refractive indices of water, hydrated collagen, and ice are 1.326,[20] ~1.43,[21] and 1.296,[22] respectively. From the Fresnel equation of reflectivity, the reflectance of normally incident light off water–ice and collagen–ice boundaries is 1% and 5%, respectively. During freezing of the water (Fig. 3), a slight increase in the subsurface OCT signal is evident in the sample due to reflectance of light at water–ice boundaries, thereby demonstrating the imaging capability of our system for Fresnel reflectance values as low as 1%.

A comparison of experiments with water (Fig. 3) and Intralipid (Fig. 4) further demonstrates the effect of local variations in refractive index on the OCT image appearance. The scattering coefficient of pure de-ionized water is negligible due to the homogeneously distributed refractive index. Thus, OCT images of water (Fig. 3) are characterized by a relatively strong surface reflectance signal and negligible subsurface signal intensity. On the other hand, Intralipid is a heterogeneous lipid suspension with a high scattering coefficient (~400 cm^{-1} at 633 nm).[15] Thus, OCT images of Intralipid (Fig. 4) have a relatively strong subsurface OCT signal. During freezing of Intralipid, subsurface changes in the OCT image are clearly evident as the freezing front approaches the air–Intralipid interface: the scattering pattern has a jagged appearance, with finger-like projections of high and low scattering regions. This solidification pattern has been observed in studies on cell freezing and is attributed to preferential freezing front propagation in directions with low solute concentrations.[23] After freezing is complete, the subsurface OCT signal is no longer present; a cue such as this might be used by the clinician as an optical marker of complete tissue freezing during cryosurgery.

Table 1 Thermal properties used in the freezing model [Eqs. (1) and (2)].

Property	Value
Density, ρ	1100 kg/m^3
Latent heat of fusion, L	336 000 J/kg
Freezing temperature, T_f	273 K
Temperature of freezing medium, T_∞	173 K
Initial temperature, T_0	303 K
Characteristic dimension, a	5×10^{-4} m
Heat transfer coefficient, h	2300 W/m^2 K
Thermal conductivity, k	0.31 W/m K
Thermal diffusivity, α	0.11 m^2/s

To assess the capability of OCT to identify freezing front boundaries, a simple model can be used to estimate the time required to freeze a given thickness of skin. The Planck equation has been used to determine freezing time for food preservation:[24]

$$t_f = \frac{\rho L}{T_f - T_\infty}\left(\frac{Pa}{h} + \frac{Ra^2}{k}\right), \quad (1)$$

where t_f is the freezing time (s), ρ is the density (kg/m^3), L is the latent heat of fusion (J/kg), T_f is the freezing temperature of the object (K), T_∞ is the freezing medium temperature (K), a is the characteristic dimension of the object, h is the heat transfer coefficient between the freezing medium and object, k is the thermal conductivity (W/m K) and P and R are constants that depend on the geometry modeled. For the semi-infinite slab geometry assumed in this model, $P = 1/2$, $R = 1/8$, and a is the object thickness [500 μm, determined from OCT images of skin in the hamster window chamber model (Fig. 5)]. Under the assumption that skin thermal properties are similar to those of water, the relevant properties are summarized in Table 1. T_∞ was selected based on measurements (described above) of the cotton-tipped applicator temperature after immersion in liquid nitrogen. h was based on measurements performed by Pikkula et al.[25] using cryogen spray cool-

ing on an epoxy skin phantom. With these thermal properties, t_f is ~0.8 s.

A limitation of this simple model is that the time required to cool the object to T_f is neglected. To estimate the minimum time required to cool skin at 500 μm depth from an initial temperature T_0 to T_f, we apply a constant surface temperature (T_f) boundary condition approximation to an analytical heat conduction model,[26] which results in the following equation:

$$T(z,t) = T_\infty + (T_0 - T_\infty)\,\mathrm{erf}\left(\frac{z}{2\sqrt{\alpha t}}\right), \qquad (2)$$

where α is the thermal diffusivity (m^2/s). With this equation, $T(z=500\ \mu m, t)$ is equal to T_f after ~1.4 s. Therefore, using Eqs. (1) and (2), the total time required for freezing a 500 μm thick layer of skin is ~2 s. From a time-resolved sequence of OCT images during the freezing of skin [Fig. 5(b)], structural changes are apparent ~6 s after application of liquid nitrogen with a cotton-tipped applicator. It is important to note that Eqs. (1) and (2) represent a simple model in which several assumptions are made, such as constant T_∞ and homogeneous thermal properties. In reality, T_∞ decreases due to heat transfer from the skin and surrounding air to the cotton-tipped applicator. Furthermore, the formation of a superficial frozen boundary layer set at $T_f = 273$ K serves to insulate deeper regions of the skin from the colder surface. Both of these factors will effectively increase the time required for freezing. Thus, the fact that the measured and predicted freezing times are on the same order of magnitude is encouraging.

In conclusion, in these studies on water, Intralipid, and *in vivo* skin, OCT was capable of imaging phase transition dynamics during freezing. For clinical use during most cryosurgery applications, OCT imaging must be done via an interstitial probe. Li et al.[27] demonstrated that OCT imaging can be performed using a 27-gauge needle inserted into the organ of interest. Using such a system might lead to percutaneous, minimally invasive, OCT monitoring of tissue freezing during cryosurgery.

Acknowledgments

The authors thank Taner Akkin and Woonggyu Jung for technical assistance with OCT imaging, Chris Rylander for his help with the experiments, and Dr. Kristen Kelly and Dr. A. J. Welch for helpful comments. This project was supported in part by research grants awarded by the National Institutes of Health to three of the authors (G.A., Grant No. HD 42057, T.E.M., Grant No. RR 14069, and J.S.N., Grant No. GM 62177). One of the authors (B.C.) acknowledges support by the Arnold and Mabel Beckman Fellows Program. Institutional support was provided by the Office of Naval Research, National Institutes of Health, and the Beckman Laser Institute and Medical Clinic Endowment.

References

1. S. E. Singletary, "Minimally invasive techniques in breast cancer treatment," *Semin Surg. Oncol.* **20**, 246–250 (2001).
2. S. O. R. Pfleiderer, M. G. Freesmeyer, C. Marx, R. Kuhne-Heid, A. Schneider, and W. A. Kaiser, "Cryotherapy of breast cancer under ultrasound guidance: Initial results and limitations," *Eur. Radiol.* **12**, 3009–3014 (2002).
3. A. A. Gage and R. P. Huben, "Cryosurgical ablation of the prostate," *Semin Urol. Oncol.* **5**, 11–19 (2000).
4. B. Nordlinger and P. Rougier, "Nonsurgical methods for liver metastases including cryotherapy, radiofrequency ablation, and infusional treatment: What's new in 2001?" *Curr. Opin. Oncol.* **14**, 420–423 (2002).
5. T. Mala, B. Edwin, E. Samset, I. Gladhaug, P. K. Hol, E. Fosse, O. Mathisen, A. Bergan, and O. Soreide, "Magnetic-resonance-guided percutaneous cryoablation of hepatic tumours," *Eur. J. Surg.* **167**, 610–617 (2001).
6. A. Kokoszka and N. Scheinfeld, "Evidence-based review of the use of cryosurgery in treatment of basal cell carcinoma," *Dermatol. Surg.* **29**, 566–571 (2003).
7. D. M. Otten, B. Rubinsky, W. F. Cheong, and D. A. Benaron, "Ice-front propagation monitoring in tissue by the use of visible-light spectroscopy," *Appl. Opt.* **37**, 6006–6010 (1998).
8. A. F. Fercher, W. Drexler, C. K. Hitzenberger, and T. Lasser, "Optical coherence tomography—Principles and applications," *Rep. Prog. Phys.* **66**, 239–303 (2003).
9. J. F. de Boer and T. E. Milner, "Review of polarization sensitive optical coherence tomography and Stokes vector determination," *J. Biomed. Opt.* **7**, 359–371 (2002).
10. B. E. Bouma and G. J. Tearney, "Clinical imaging with optical coherence tomography," *Acad. Radiol.* **9**, 942–953 (2002).
11. J. G. Fujimoto, C. Pitris, S. A. Boppart, and M. E. Brezinski, "Optical coherence tomography: An emerging technology for biomedical imaging and optical biopsy," *Neoplasia* **2**, 9–25 (2000).
12. Z. P. Chen, Y. H. Zhao, S. M. Srinivas, J. S. Nelson, N. Prakash, and R. D. Frostig, "Optical Doppler tomography," *IEEE J. Sel. Top. Quantum Electron.* **5**, 1134–1142 (1999).
13. J. M. Schmitt, "Optical coherence tomography (OCT): A review," *IEEE J. Sel. Top. Quantum Electron.* **5**, 1205–1215 (1999).
14. J. T. Walsh, Jr. and T. F. Deutsch, "Pulsed CO_2 laser tissue ablation: Measurement of the ablation rate," *Lasers Surg. Med.* **8**, 264–275 (1988).
15. S. T. Flock, S. L. Jacques, B. C. Wilson, W. M. Star, and M. J. C. van Gemert, "Optical properties of Intralipid: A phantom medium for light propagation studies," *Lasers Surg. Med.* **12**, 510–519 (1992).
16. Z. F. Gourgouliatos, A. J. Welch, and K. R. Diller, "Microscopic instrumentation and analysis of laser–tissue interaction in a skin flap model," *J. Biomech. Eng.* **113**, 301–307 (1991).
17. S. Mordon, T. Desmettre, J. M. Devoisselle, and V. Mitchell, "Selective laser photocoagulation of blood vessels in a hamster skin flap model using a specific ICG formulation," *Lasers Surg. Med.* **21**, 365–373 (1997).
18. J. K. Barton, G. Vargas, T. J. Pfefer, and A. J. Welch, "Laser fluence for permanent damage of cutaneous blood vessels," *Photochem. Photobiol.* **70**, 916–920 (1999).
19. G. Vargas, K. F. Chan, S. L. Thomsen, and A. J. Welch, "Use of osmotically active agents to alter optical properties of tissue: Effects on the detected fluorescence signal measured through skin," *Lasers Surg. Med.* **29**, 213–220 (2001).
20. A. G. Van Engen, S. A. Diddams, and T. S. Clement, "Dispersion measurements of water with white-light interferometry," *Appl. Opt.* **37**, 5679–5686 (1998).
21. X. J. Wang, T. E. Milner, M. C. Chang, and J. S. Nelson, "Group refractive index measurement of dry and hydrated type I collagen films using optical low-coherence reflectometry," *J. Biomed. Opt.* **1**, 212–216 (1996).
22. S. G. Warren, "Optical constants of ice from the ultraviolet to the microwave," *Appl. Opt.* **23**, 1206–1223 (1984).
23. B. Rubinsky, "Microscale heat transfer in biological systems at low temperatures," *Exp. Heat Transfer* **10**, 1–29 (1997).
24. Q. T. Pham, "Extension to Planck's equation for predicting freezing times of foodstuffs of simple shapes," *Int. J. Refrig.* **7**, 377–383 (1984).
25. B. M. Pikkula, J. W. Tunnell, and B. Anvari, "Methodology for characterizing heat removal mechanism in human skin during cryogen spray cooling," *Ann. Biomed. Eng.* **31**, 493–504 (2003).
26. F. P. Incropera and D. P. DeWitt, *Fundamentals of Heat and Mass Transfer* (Wiley, New York, 1996).
27. X. D. Li, C. Chudoba, T. Ko, C. Pitris, and J. G. Fujimoto, "Imaging needle for optical coherence tomography," *Opt. Lett.* **25**, 1520–1522 (2000).